

This is a repository copy of *An accurate description of Aspergillus niger organic acid batch fermentation through dynamic metabolic modelling*.

White Rose Research Online URL for this paper:

<https://eprints.whiterose.ac.uk/124196/>

Version: Accepted Version

Article:

Upton, Daniel John, McQueen Mason, Simon John orcid.org/0000-0002-6781-4768 and Wood, Andrew James orcid.org/0000-0002-6119-852X (2017) An accurate description of *Aspergillus niger* organic acid batch fermentation through dynamic metabolic modelling. *Biotechnology for biofuels*. 258. ISSN 1754-6834

<https://doi.org/10.1186/s13068-017-0950-6>

Reuse

Items deposited in White Rose Research Online are protected by copyright, with all rights reserved unless indicated otherwise. They may be downloaded and/or printed for private study, or other acts as permitted by national copyright laws. The publisher or other rights holders may allow further reproduction and re-use of the full text version. This is indicated by the licence information on the White Rose Research Online record for the item.

Takedown

If you consider content in White Rose Research Online to be in breach of UK law, please notify us by emailing eprints@whiterose.ac.uk including the URL of the record and the reason for the withdrawal request.

Biotechnology for Biofuels

An accurate description of *Aspergillus niger* organic acid batch fermentation through dynamic metabolic modelling

--Manuscript Draft--

Manuscript Number:	BBIO-D-17-00324	
Full Title:	An accurate description of <i>Aspergillus niger</i> organic acid batch fermentation through dynamic metabolic modelling	
Article Type:	Research	
Section/Category:	Fungal/yeast genetics, physiology and metabolic engineering	
Funding Information:	Biotechnology and Biological Sciences Research Council (BB/J014443/1)	Mr Daniel Upton
Abstract:	<p>Background</p> <p><i>Aspergillus niger</i> fermentation has provided the chief source of industrial citric acid for over 50 years. Traditional strain development of this organism was achieved through random mutagenesis, but advances in genomics have enabled development of genome-scale metabolic modelling that can be used to make predictive improvements in fermentation performance. The parent citric acid producing strain of <i>A. niger</i>, ATCC 1015, has been described previously by a genome-scale metabolic model that encapsulates its response to ambient pH. Here, we report the development of a novel double optimisation modelling approach that generates time-dependent citric acid fermentation using dynamic flux balance analysis.</p> <p>Results</p> <p>The output from this model shows a good match with empirical fermentation data. Our studies suggest that citric acid production commences upon a switch to phosphate-limited growth and this is validated by fitting to empirical data, which confirms the diauxic growth behaviour and the role of phosphate storage as polyphosphate.</p> <p>Conclusions</p> <p>The calibrated time-course model reflects observed metabolic events and generates reliable in silico data for industrially relevant fermentative time series, and for the behaviour of engineered strains suggesting that our approach can be used as a powerful tool for predictive metabolic engineering.</p>	
Corresponding Author:	Daniel Upton University of York UNITED KINGDOM	
Corresponding Author Secondary Information:		
Corresponding Author's Institution:	University of York	
Corresponding Author's Secondary Institution:		
First Author:	Daniel Upton	
First Author Secondary Information:		
Order of Authors:	Daniel Upton	
	Simon McQueen-Mason	
	Andrew Jamie Wood	
Order of Authors Secondary Information:		

An accurate description of *Aspergillus niger* organic acid batch fermentation through dynamic metabolic modelling

Daniel J. Upton¹, Simon J. McQueen-Mason¹, A. Jamie Wood^{1,2}

Author details:

Author 1: Daniel John Upton

Email address: dju500@york.ac.uk

Author 2: Simon John McQueen-Mason

Email address: simon.mcqueenmason@york.ac.uk

Author 3: Andrew Jamie Wood

Email address: jamie.wood@york.ac.uk

Institutional addresses:

1. Department of Biology, University of York, Wentworth Way, York, YO10 5DD, United Kingdom

2. Department of Mathematics, University of York, Heslington, York, YO10 5DD, United Kingdom

Correspondence to A. Jamie Wood

Abstract

Background

Aspergillus niger fermentation has provided the chief source of industrial citric acid for over 50 years. Traditional strain development of this organism was achieved through random mutagenesis, but advances in genomics have enabled development of genome-scale metabolic modelling that can be used to make predictive improvements in fermentation performance. The parent citric acid producing strain of *A. niger*, ATCC 1015, has been described previously by a genome-scale metabolic model that encapsulates its response to ambient pH. Here, we report the development of a novel double optimisation modelling approach that generates time-dependent citric acid fermentation using dynamic flux balance analysis.

Results

The output from this model shows a good match with empirical fermentation data. Our studies suggest that citric acid production commences upon a switch to phosphate-limited growth and this is validated by fitting to empirical data, which confirms the diauxic growth behaviour and the role of phosphate storage as polyphosphate.

Conclusions

The calibrated time-course model reflects observed metabolic events and generates reliable *in silico* data for industrially relevant fermentative time series, and for the behaviour of engineered strains suggesting that our approach can be used as a powerful tool for predictive metabolic engineering.

Keywords: *Aspergillus niger*; citric acid; dFBA; metabolic modelling; polyphosphate

Background

Due to its natural ability to secrete organic acids and proteins, the filamentous fungus *Aspergillus niger* is an established organism for the industrial production of citric acid and enzymes. *A. niger* is metabolically highly versatile, a feature that has made it useful for a wide range of biotechnological biotransformations [1]. *A. niger* also produces a wide range of secondary metabolites, with over 100 reported to date [2]. *A. niger* is a saprotroph and its natural habitat is soil, although it can be found in wide-ranging habitats, such as rotting fruit, plant debris, and indoor environments. This fast-growing fungus is both acid- and thermo-tolerant, able to grow in the pH range 1.4-9.8 and in the temperature range 6-47°C [3]. This versatility and its ease of culture has helped it become an established industrial organism. Its haploid genome is around 35 Mb in size with 8 chromosomes which contain about 12,000 genes, 57% of which have functional assignments [4]. Aspergilli are an important and diverse group, which in addition to *A. niger*, include well-studied species such as the model genetic organism *A. nidulans*, the pathogen *A. fumigatus* and the domesticated *A. oryzae*. Full genome sequences are currently available for 18 species of the Aspergilli group [5] and some of these have been subject to extensive systems biology studies [6].

With global production of 2 million tonnes a year, citric acid is an industrial chemical with many applications [7]. Its main use is in the food and drinks industry, but is also used in cleaning agents, pharmaceuticals, animal feed, and metal cleaning [8]. Industries using *A. niger* fermentation are dependent on sucrose-based feedstocks,

but with rising costs and increasing concerns over food security, a switch to more sustainable and lower cost feedstocks is desirable [9]. *A. niger* can assimilate a wide range of carbon sources, and therefore has great potential for exploiting underused resource streams such as pentose sugars from lignocellulose.

The best industrial strains are capable of producing over 70% of the theoretical yield of citric acid [10]. Such strains have been developed over many decades by time-consuming random mutagenesis. The genotype of resulting strains remains unknown, and random mutagenesis can lead to genetic instability of developed strains. Rational engineering of *A. niger* is now feasible, particularly with advances in genomics over recent years that have paved the way for genome-scale metabolic modelling [5, 11]. Industrially, *A. niger* is utilised via large-scale batch fermentations rather than continuous culture methods, typically in reactors in excess of 100,000 litres [12]. In order for genome-scale models to accurately capture the behaviour of these cultures, techniques which model the batch growth, rather than simple chemostat-like cultures, are required.

The genome of the parent citric acid producing strain of *A. niger*, ATCC 1015, has been sequenced [4]. This enabled development of the genome-scale metabolic model for *A. niger*, MA871, which reflects ATCC 1015 metabolism [13]. The model was further developed to reflect the well-known behaviour of *A. niger* to acidify its surroundings in response to ambient pH [14]. This was achieved by incorporating acid-dissociation reactions for seven organic acids reportedly secreted by *A. niger*.

Each reaction gives the number of protons released by a particular acid as a function of ambient pH. Citric acid production was modelled statically using flux balance analysis (FBA). The objective function was either set to proton production at a fixed growth rate or proton production was incorporated into the biomass equation. The nature of organic acid production in response to ambient pH is, however, a dynamic one, with acid-dissociation reactions changing as protons are produced.

In this article, we further develop the *A. niger* metabolic model to take into account the dynamic nature of organic acid production. By designing a novel modelling approach that employs dynamic flux balance analysis (dFBA), we demonstrate a model that gives time-course fermentative series of citric acid production. We validate the new model by fitting to empirical data from ATCC 1015 citric acid fermentations, and demonstrate how the resultant time-course calibrated model can be used as a powerful platform for metabolic engineering of *A. niger*.

Results

Citric acid fermentation occurs as part of a diauxic growth response

To investigate citric acid production by the parent citric acid producing ATCC 1015 strain, empirical time course data were obtained from fermentation performed in shake flasks. Biomass and citric acid production were monitored with samples taken at 24 hour time-points. Diauxic growth behaviour was observed, with a drop in growth rate at day 3 (Fig 1A). Citric acid production commenced at day 3, coinciding with the diauxic growth shift (Fig 1B). 60 g/L citric acid was produced.

116

117 In order to better understand the basis of this growth behaviour we developed a
118 dynamic flux balance analysis (dFBA) model based on the previously published FBA
119 model [13, 14]. To validate the model and further investigate the diauxic growth
120 behaviour, empirical data were obtained for citric acid fermentation under a range of
121 phosphate levels (0.05, 0.09 and 0.17 g/L). Samples of the cultures were taken
122 every 24 hours to produce a time-course of biomass dry weight, phosphate
123 depletion, citric acid production, and glucose consumption (Fig 2). Phosphate was
124 rapidly taken up and depleted by day 2 (Fig 2B), yet growth continued (Fig 2A).
125 Phosphate was therefore clearly stored internally to enable growth during absence of
126 external phosphate. Diauxic growth was observed, with growth becoming phosphate-
127 limited. The diauxic growth shift was synchronous with depletion of external
128 phosphate. The phosphate-limited growth rate was a function of the initial phosphate
129 concentration, with increased growth rate at higher phosphate. The timing of citric
130 acid production was observed to coincide with the onset of phosphate-limited growth
131 and external phosphate depletion (Fig 2C). Up to 50 g/L citric acid was produced,
132 with the culture at 0.17 g/L phosphate producing the most. Glucose uptake was
133 relatively slow for the lower phosphate cultures and a limiting factor in citric acid
134 production (Fig 2D).

135

136 From these observations, we hypothesised that the diauxic growth shift is caused by
137 a switch to phosphate-limited growth, resulting in citric acid production. This
138 hypothesis was motivated by examination of our data, existing knowledge of *A. niger*

[10] and also the ecological evidence that organic acids are released extracellularly in order to facilitate the mobilisation of phosphate, especially in soil [15]. We decided to examine the plausibility of this hypothesis using dFBA modelling.

Simulating citric acid fermentation by dynamic flux balance analysis

To create time-course simulations comparable to the citric acid fermentation empirical data, dynamic flux balance analysis (dFBA) was used with the *MA871* metabolic model [13]. Citric acid production was modelled by incorporating kinetic acid-dissociation reactions into the dFBA schema for the organic acids in *MA871* and setting the objective to proton production. This explicit inclusion leads to an acid hierarchy [14], which suggested that citric acid production was the most efficient means of acidification with oxalic acid production switched off.

In the standard setting for the metabolic model citric acid secretion is included as a part of the external constraints during growth [13]; however, this is not supported by our observations. Therefore, a novel modelling approach was designed to simulate the diauxic growth behaviour with citric acid production commencing upon a diauxic growth shift coupled to phosphate intake. To achieve this, a double optimisation dFBA setup was designed (Fig 3). The objective is first set to biomass production, with the maximised growth rate then used in the second optimisation. The second objective is dependent on the growth-limiting condition of the first optimisation. The decision process uses a boolean expression. If the external phosphate flux is lower than its flux constraint, the second objective is set to phosphate storage to store

excess phosphate not used for growth. Otherwise, external phosphate flux is equal to its flux constraint and the second objective is set to proton production to make use of the carbon not used for growth (phosphate-limited growth).

The dynamic modelling approach, dFBA, therefore includes a number of metabolite pools that are tracked outside of the FBA, including external glucose, external phosphate, external pH, organic acids as well as the hypothesised stored phosphate. These metabolite pools are linked to the FBA simulations at each step via first order differential equations describing transport processes. These differential equations are solved at each time-step to provide flux constraints for the FBA optimisations occurring in a tandem fashion and assuming the metabolic system remains at a steady-state despite the small changes in the external constraints. All equations used are detailed in the methods, but are essentially either linear diffusion or Michaelis-Menten transport equations across the membrane as described below and mathematically in the methods section. Literature sources were used to parameterise the model wherever available as described below.

Following previous studies [16, 17], glucose uptake was modelled as the sum of passive diffusion and facilitated diffusion, using empirical values from the literature [16, 17] for all transport-mediated kinetic parameters (Table 2). The calculated parameter for passive diffusion overestimated glucose uptake, and therefore was fitted to empirical data (Table 1). Transport-mediated glucose uptake in *A. niger* is inhibited by low pH and non-competitively inhibited by external citrate [17], and this

was therefore included in the modelled glucose uptake. *A. niger* has both low- and high-affinity glucose transport systems [17], both of which were included in the model. The low-affinity system is reported only active above 150 g/L glucose, [17] and so this system was only included in the model at high glucose (>150 g/L).

Phosphate uptake and release of stored phosphate were modelled according to Michaelis-Menten kinetics. As no characterised phosphate transporters could be found for *A. niger* in the literature, kinetic parameters were fitted to empirical data on phosphate uptake (Table 1).

Fitting of model parameters to empirical data and model validation

The empirical data obtained from the experiment varying phosphate were used to fit model parameters and validate the model. A total of eight parameters were fitted to a data-set containing 84 data-points. As each data-point was in quadruplicate with very low error margins, we decided to use the data-set for both model training and validation. The trained model was later applied to independent data-sets (Fig 4), which gave further validation. Using the trained model, citric acid fermentation was simulated for each of the phosphate levels tested, and model predictions plotted alongside empirical data (Fig 2). The modelled diauxic growth behaviour gave good fits to empirical data, with external phosphate depletion being the trigger that results in phosphate-limited growth and citric acid production. All the model outputs showed a strong qualitative comparison to the empirical data with unfitted parameters taken directly from the literature. Notably the modelled glucose uptake fitted empirical data

208 closely (Fig 2D) with unadjusted literature values for transport-mediated uptake rate
209 and affinity.

210
211 However, a number of adjustments were required for the model to fit the empirical
212 data more closely. In particular, the model underestimated biomass production
213 during phosphate-limited growth, suggesting a lower phosphate demand not
214 reflected in the MA871 biomass equation. These contrasting observations in the
215 different areas of growth suggest that the biomass equation for the MA871 model
216 represents an average biomass composition over different growth conditions and
217 that therefore the biomass equation needs to be altered. Differences in biomass
218 composition in different growth conditions have previously been reported in
219 *Escherichia coli* [18]. To reflect citric acid producing conditions, two new fitted
220 parameters were added to the model, the nucleic acid and phospholipid components
221 of the biomass equation (Supplementary Table S1). The ratios between the different
222 components of each, and the total mass of the biomass components were kept
223 constant. Change in mass was balanced by adjustment of the glycerol component,
224 which has been reported to increase during citric acid producing conditions [19]. The
225 additional parameters increase the complexity of the model, and the likelihood of
226 overfitting. Therefore, Akaike Information Criterion (AIC) [20] was used to measure
227 the quality of fit and assess improvement in the model (Table 4) (see Methods).

228
229 Our model initially overestimated citric acid production. This may be due to the many
230 internal constraints imposed on the internal metabolism by the intracellular

accumulation of, or simply high throughputs of citrate that are not accounted for by the steady-state methodology of flux balance analysis. For example, the citrate sensitivity of 6-phosphofructo-1-kinase is a target of attempts to increase citrate production [21] and the rates of mitochondrial citrate export [22] and citrate secretion may be limiting. To reflect these constraints a limit to the citric acid output rate, v_{CIT} , was added and fitted as a parameter to more closely reflect empirical data (Table 1). Carbon uptake was decreased slightly as a result of the constraint on citric acid output, but still gave close fits to empirical data. The new model was assessed by calculating the AIC (see Methods), which showed a significant improvement (Table 4).

Citric acid production on other carbon sources

To further investigate the diauxic growth behaviour, we tested citric acid fermentation using D-xylose as a substrate at an initial concentration of 160 g/L. The same diauxic growth shift coupled citric acid response was seen with xylose (Fig 4) as seen with glucose. We applied our model, with previously fitted parameters unchanged. The empirical data from this experiment was not used in previous model training, and served to provide further validation with glucose as substrate and at a different phosphate level. The uptake rate of xylose was modelled similarly to glucose as the sum of passive and facilitated diffusion. The kinetic parameters for xylose uptake were fitted to our empirical data (Table 1). Close fits were achieved for biomass production and carbon source consumption, demonstrating the wide applicability of the dynamic model. Citric acid production was overestimated by the model, which

may suggest a further limiting factor with xylose as the carbon source. The constraint applied to citric acid output rate, v_{CIT} , was the same as for glucose (Table 1). The discrepancy may be due to differing morphology as we observed decreased biomass pellet sizes and higher viscosity in cultures grown on xylose.

Investigating the role of phosphate during citric acid fermentation

As growth on glucose continued beyond external phosphate depletion (Fig 2B), it became clear that *A. niger* has a phosphate storage mechanism, possibly via accumulation of polyphosphate as previously reported [23]. To investigate this, polyphosphate was extracted from biomass grown under citric acid producing conditions and quantified. Polyphosphate levels were observed to rise early on in fermentation, peaking at day 2 at the point of external phosphate depletion (Fig 5). Polyphosphate levels dropped rapidly from day 2 to day 4, with a more gradual decrease later in fermentation coinciding with phosphate-limited growth and citric acid production.

To further investigate the importance of phosphate, we searched for the genes encoding phosphate transporters in *A. niger* ATCC 1015. A total of 8 putative genes were found (based on similarity to known transporters), suggesting *A. niger* has evolved a range of phosphate uptake mechanisms as adaptation to different environmental conditions (Supplementary Table S2). It may be that only a subset of these genes encode phosphate transporters while others encode phosphate sensors. One of the genes (accession number EHA22558) has clear homologues in

other species (Fig S1), but none of these have been characterised or parameterised at the level of protein activity. The other gene annotations are more speculative so may not encode phosphate transporters [24].

The dFBA model provides a platform for predictive metabolic engineering

A prediction of the model is that oxalic acid production is the most efficient means of acidification at initial pH 7, followed by citric acid. It is well known that *A. niger* predominantly secretes oxalic and gluconic acid at higher initial pH and that by imposing a low initial pH during fermentation, production of these competing organic acids is prevented and citric acid production is increased [14]. Our model suggests that by switching off oxalic acid production by deletion of oxaloacetate hydrolase (oah), citric acid will solely be produced. The model does not predict gluconic acid production suggesting this may be decoupled from proton production and is instead a means of quickly sequestering glucose, through the action of extracellular glucose oxidase, early in fermentation.

To investigate this phenomenon, we engineered the ATCC 1015 strain by targeted gene deletion strategies to knockout oah and the gene encoding glucose oxidase (gox) responsible for gluconic acid production. We created two single knockouts (Δ oah and Δ gox) and a double knockout (Δ oah Δ gox), and characterised citric acid fermentation by these knockout strains at initial pH 7 (Fig 6). Citric acid yield was significantly increased in the Δ oah strain with a further marginal improvement in Δ oah Δ gox. This was not the case for the Δ gox strain suggesting gluconic acid

production occurs independently of proton production without impacting citric acid fermentation. Gluconic acid was produced early in fermentation while oxalic and citric acid production occurred later. The synchronicity of oxalic and citric acid production suggests they are part of the same proton production response. In this experiment, the Mn^{2+} concentration was increased to 1000 ppb. Citric acid production usually requires Mn^{2+} -deficient media, though was previously reported insensitive to Mn^{2+} in an oah and gox double negative mutant strain at pH 5 [25]. The presence of Mn^{2+} did not prevent citric acid production at initial pH 7, suggesting that its effect is limited to low pH conditions.

We applied our dFBA model to the Δoah and Δgox knockouts at initial pH 7, which gave close fits for oxalic and gluconic production. The differences in predicted citric acid production between the knockout strains showed a qualitative fit with empirical data (Fig 6). However, constraints on oxalic and citric acid output rates, v_{OXAL} and v_{CIT} respectively (Table 1), were required to achieve the close fits. The constraint on citric acid output rate, v_{CIT} , was different to that applied at initial pH 2. This may be due to morphological differences as we observed increased biomass pellet sizes when *A. niger* was grown at higher initial pH. The impact of differing morphology on transport processes and on anaerobicity within pellets requires further investigation. The widely reported absence of oxalic acid production below pH 2 [10, 25] was implemented in the model to reflect empirical data. To simulate gluconic acid production, the flux of the extracellular GOX and gluconic acid dissociation reactions were forced dependent on GOX kinetic parameters and the ambient pH. The kinetic

parameters V_{\max} and K_M of GOX (Table 2) were taken from the literature [26, 27].

The concentration of GOX per gram biomass dry weight is unknown for these experimental conditions so was fitted to empirical data (Table 1). The proportion of active GOX was based on empirical data of GOX activity at varying pH [28].

Discussion

We have developed a novel dynamic model of *A. niger* citric acid fermentation that employs dFBA, to give time-course simulations of batch fermentation relevant to the industrial and experimental modes of *A. niger* fermentation. Our physiologically motivated double optimisation approach is a novel use of dFBA. Previous work incorporated proton production into the MA871 metabolic model and used FBA in a static manner to give predictions on organic acid production [13, 14] at fixed values of pH. Since acid dissociation reactions are dependent on the dynamic ambient pH, the application of dFBA with the dynamic tracking of pH enables more accurate predictions on organic acid production. The dynamic model was also expanded to include alternative feedstocks. Xylose was chosen as it is a pentose sugar abundant in hemicellulose in plant biomass and readily metabolised by *A. niger*. This new dynamic model is therefore a valuable addition to the *A. niger* metabolic modelling toolbox and a powerful demonstration of the promise of dFBA for applications in industrial biotechnology.

We tested the ability of the model to predict the impact of genetic modifications on organic acid fermentation at higher initial pH. We deleted genes encoding

oxaloacetate acetylhydrolase (oah) and glucose oxidase (gox) to eliminate oxalic and gluconic production respectively. Deletion of oah significantly increased citric acid production, and this was also observed in model predictions, though less pronounced. This suggests that the presence of oxalic acid in the cytosol in the oah positive strains may have negating effects on citric acid production not reflected by the model. It is expected that cytosolic organic acid accumulation may occur as a result of constrained transport, which is likely to have regulatory effects on organic acid production as a safeguard mechanism.

A. niger has been an industrial workhorse for decades and is essential to the world's citric acid production. This is achieved through batch or fed-batch fermentation and the new model enables simulation of the dynamic process for the first time. The underlying causes of the naturally evolved property of organic acid production are still unclear. It was previously reported through static FBA predictions [14] that this may be driven by the biological objective of proton production. In line with empirical findings, oxalic acid production was revealed as the most efficient means of proton production at wide ranging pH with citric acid second at low pH. We have now shown this in a dynamic manner with variable external pH taken into account. Empirical data revealed that oxalic and citric acid production are synchronous upon a switch to phosphate-limited growth. This suggests they are coupled and part of the same proton production response. This is further supported by the significant increase in citric acid production in Δoah .

369 The role of phosphate is striking as organic acid secretion has been reported in *A.*
370 *niger* and other organisms as a phosphate mobilisation strategy [15, 29, 30]. The
371 observed phosphate-limited growth results from the ability of *A. niger* to rapidly take
372 up phosphate and store it as polyphosphate. The constraint on polyphosphate
373 hydrolysis then limits growth, enabling flux of carbon to organic acid production.
374 While *A. niger* has sufficient stored phosphate for growth, it does not use it and
375 keeps it reserved. This behaviour may be due to the energy storage value of
376 polyphosphate. We have observed a release of phosphate late in fermentation upon
377 carbon depletion, which suggests *A. niger* is capable of rapid polyphosphate
378 hydrolysis as a means to create ATP when other energy sources are limiting. The
379 control mechanisms that exist in *A. niger* to regulate polyphosphate hydrolysis and
380 their relation to organic acid production warrant further investigation.
381
382 Our modelling approach has further demonstrated the potential of dFBA; the
383 augmentation of static steady state FBA by dynamic transport processes and time
384 varying pools of metabolites. It has also revealed some fundamental issues with the
385 application of these techniques to real applications. The objective function – the
386 biomass equation – is fundamental to FBA and is typically constructed with evidence
387 from mass spectrometry. Our work suggests that this function is strongly dependent
388 on the fermentation context and may even be variable over the growth process.
389 Biologically this is highly plausible, but dramatically increases the complexity of
390 model implementation and fitting. In addition, it is clear that important regulatory
391 constraints on the metabolic process, in this case citrate accumulation, need to be

included. In this manner, we have created an augmented dFBA model in a potentially grey area between a complete kinetic model and the genetically based simplicity of an FBA model. Further work is required to fully understand validity of such models.

Conclusions

Our findings reveal a naturally evolved behaviour that has been exploited by industry for decades to produce citric acid. Our work, encapsulated in a dynamic model, further elucidates the causative factors in organic acid fermentation by *A. niger* exploited by industrial processes. The model provides a means to further probe this behaviour and accurately explore the effects of genetic changes on organic acid fermentation in a dynamic manner. This new addition to the *A. niger* systems biology toolbox paves the way for metabolic engineering efforts to create new strains capable of enhanced citric acid production on low-cost feedstocks.

Methods

Shake flask experiments

Citric acid fermentation experiments were performed in 250 ml DeLong neck baffled shake flasks (Bellco Glass Inc.; Vineland, NJ, USA) with 30 ml medium. Flasks were siliconized with 2% (v/v) dimethyldichlorosilane. Cultures were incubated at 30°C with shaking at 250 rpm. The following medium was used: glucose (160 g/L), urea (3.6 g/L), (NH₄)₂SO₄ (0.52 g/L), K₂HPO₄ (0.5 g/L), CaCO₃ (0.03125 g/L), MgSO₄·7H₂O (0.275 g/L), ZnSO₄·7H₂O (0.00225 g/L), FeSO₄·7H₂O (0.0095 g/L),

CuSO₄·5H₂O (0.0117 g/L), MnCl₂·(H₂O)₄ (0.0000108 g/L), citric acid monohydrate (3.3 g/L), Tween 80 (0.0094%). The Mn²⁺ concentration was confirmed as 7 ppb by ICP-MS (Biorenewables Development Centre, York, UK). The medium was autoclaved (121°C 15 minutes) excluding glucose which was filter sterilised (0.22 µm). The pH of the medium was adjusted after autoclaving by addition of sterile 2 M H₂SO₄. The medium included 10 mM uridine in experiments using pyrG negative strains. The medium was inoculated with 1×10⁶ spores/ml. Spores were harvested from potato dextrose agar slants incubated for 2 days at 37°C. 2 ml saline Tween (0.1% Tween 80, 9 g/L NaCl) was added per slant and shaken to disperse spores. Spores were washed 3 times in saline Tween. 500 µl samples of cultures were taken every 24 hours for determination of biomass, metabolites and phosphate. Samples were collected in pre-dried, pre-weighed 1.5 ml Eppendorf tubes and centrifuged at 9000 g for 5 minutes. The supernatant was retained for metabolite analysis and phosphate determination and stored at -20°C.

Biomass dry weight determination

Mycelia were washed 4 times in 1 ml dH₂O and centrifuged at 9000 g for 5 minutes. Biomass was dried at 70°C to constant weight. Biomass dry weight was determined by subtracting weight of the pre-dried 1.5 ml Eppendorf tube.

Metabolite analysis

Enzymatic assay kits were used to determine the level of metabolites. Glucose, citric acid, xylose, glycerol and gluconic acid were determined using Megazyme assay kits

(K-GLUC, K-CITR, K-XYLOSE, K-GCROLGK, and K-GATE respectively)

(Megazyme International Ireland Ltd., Wicklow, Ireland). Oxalic acid was determined using the LIBIOS oxalate assay kit (Oxalate-100; LIBIOS, France).

Phosphate determination

Phosphate was determined by the ammonium molybdate method, using an assay kit (ab65622; Abcam, Cambridge, UK).

Polyphosphate extraction and quantification

Mycelia were grown up in shake flasks using the same method as previously described. Mycelia were harvested at 8 time-points (days 1 to 8) in triplicate. To obtain sufficient biomass, one flask was harvested per sample. Day 1 samples required the pooling of 4 flasks per replicate. Mycelia were harvested using a double layer of Miracloth (Calbiochem) and washed in 300 ml ice-cold 100 mM Tris.HCl pH 7 followed by 600 ml ice-cold dH₂O. Washed mycelia were transferred to 15 ml Falcon tubes, flash frozen in liquid nitrogen, freeze dried, and stored at -80°C. Freeze dried mycelia were weighed out in 2 ml vials, approximately 50 mg per vial. Biomass was ground using the TissueLyser II (QIAGEN; Crawley, UK) at 30 Hz for 90 seconds 3 times. Each vial contained 2 beads. Powdered mycelia were lysed by adding 2 ml 10% (w/v) lysing enzymes from *Trichoderma harzianum* (Sigma, Dorset, UK) and incubating at 30°C with shaking for 3 hours. Samples were centrifuged and supernatant discarded. Polyphosphate was extracted following a previously described protocol [23]. All centrifuge steps were done at 13,000 rpm for 10 minutes

at 4°C and all shaking was done at 30 rpm. The polyphosphate fraction was dried in a Savant SPD131DDA SpeedVac Concentrator (Thermo Fisher Scientific). Polyphosphate was quantified by measuring free phosphate before and after acid hydrolysis using the previously described phosphate determination method. Acid hydrolysis was performed by adding 2 ml 0.5 M H₂SO₄ to the dry pellet and boiling at 100°C for 3 hours.

Dynamic modelling of organic acid fermentation

Modelling was performed using the MA871 metabolic model [13] as the model for the flux balance analysis. During this project, a more complete model of *A. niger* metabolism was published [31] but as this retains the core of MA871 and is not specific to ATCC 1015 we have not adopted this model. The FBA calculations were performed using bespoke Java code which implements the GLPK toolkit (GNU). dFBA routines were written directly into the Java code with the differential equations solved by simple time-stepping (Euler method) with small values for the time-step. The ODEs (ordinary differential equations) were solved according to

$$C_{n+1} = C_n + t f_n B_n, \quad (1)$$

where C_{n+1} is the mmol of compound at time-point n+1, C_n is the mmol of compound at time-point n, t is the time-step (1/60 h), f_n is the flux (mmol gDW⁻¹ h⁻¹) at time-point n, and B_n is the biomass (gDW) at time-point n. The flux constraints at time-point n+1 were calculated by the following kinetic equations. External phosphate input (P_{le}) was constrained according to

$$v_{Pe} = \frac{v_{Pe,max} P_e}{K_{Pe} + P_e}, \quad (2)$$

where v_{pe} is the external phosphate uptake rate (mmol gDW⁻¹ h⁻¹) and P_e is the external phosphate concentration (mM).

Internal phosphate input (PI \rightleftharpoons) was constrained according to

$$v_P = \frac{v_{P,max}P}{K_P + P}, \quad (3)$$

where v_P is the internal phosphate input rate (mmol gDW⁻¹ h⁻¹) and P is the concentration of stored phosphate (mM).

If external glucose was below 150 g/L, external glucose uptake (DGLCe \rightleftharpoons DGLC) was constrained according to

$$v_G = v_{G1}G + \frac{v_{G2,max}G}{K_{G2}\left(1+\frac{C}{K_{i2}}\right)+G\left(1+\frac{C}{K_{i2}}\right)}, \quad (4)$$

where v_G is the external glucose uptake rate (mmol gDW⁻¹ h⁻¹), G is the external glucose concentration (mM), and C is the external citrate concentration (mM).

If external glucose was greater than or equal to 150 g/L, external glucose uptake was constrained according to

$$v_G = v_{G1}G + \frac{v_{G2,max}G}{K_{G2}\left(1+\frac{C}{K_{i2}}\right)+G\left(1+\frac{C}{K_{i2}}\right)} + \frac{v_{G3,max}G}{K_{G3}\left(1+\frac{C}{K_{i3}}\right)+G\left(1+\frac{C}{K_{i3}}\right)}, \quad (5)$$

where v_G is the external glucose uptake rate (mmol gDW⁻¹ h⁻¹), G is the external glucose concentration (mM), and C is the external citrate concentration (mM).

If external xylose was below 150 g/L, external xylose uptake (XYLe \rightleftharpoons) was constrained according to

$$v_X = v_{X1}X + \frac{v_{X2,max}X}{K_{X2}+X}, \quad (6)$$

505 where v_X is the external xylose uptake rate ($\text{mmol gDW}^{-1} \text{h}^{-1}$), and X is the external
506 xylose concentration (mM).

507 If external xylose was greater than or equal to 150 g/L, external xylose uptake was
508 constrained according to

$$v_X = v_{X1}X + \frac{v_{X2,max}X}{K_{X2}+X} + \frac{v_{X3,max}X}{K_{X3}+X}, \quad (7)$$

510 where v_X is the external xylose uptake rate ($\text{mmol gDW}^{-1} \text{h}^{-1}$), and X is the external
511 xylose concentration (mM).

512 The extracellular GOX (glucose oxidase) reaction rate was calculated according to,

$$v_{GOX} = p_{GOX} \frac{v_{GOX,max}G}{K_{GOX}+G}, \quad (8)$$

514 where v_{GOX} is the GOX reaction rate, p_{GOX} is the proportion of active GOX, and G is
515 the external glucose concentration (mM).

516 The proportion of active GOX, p_{GOX} , as a function of pH was determined according
517 to,

$$p_{GOX} = -0.102pH^2 + 1.082pH - 1.95 \quad (9)$$

519 The kinetic parameters were either fitted to our empirical data (Table 1) or set to
520 empirical values from the literature if available (Table 2).

521

522 The MA871 model was adapted to include proton production as an objective
523 function and acid-dissociation reactions for seven acids (citric, oxalic, gluconic,
524 acetic, malic, succinic, lactic) but as a function of a dynamic external pH rather than
525 a fixed pH [14]. The number of protons released in each acid-dissociation reaction
526 was calculated at each time-step according to the following equation based on
527 ambient pH and pKa values.

$$H = \frac{K_1(H_e)^{-1} + 2K_1K_2(H_e)^{-2} + 3K_1K_2K_3(H_e)^{-3}}{1 + K_1(H_e)^{-1} + K_1K_2(H_e)^{-2} + K_1K_2K_3(H_e)^{-3}}, \quad (10)$$

where K_1 , K_2 , and K_3 are constants calculated from pKa values of each acid species (Table 3), and H_e is the external molar concentration of protons that is tracked in the dFBA as a dynamic pool.

An output reaction was added for external protons ($H_{pe} \rightleftharpoons$), which was set as the objective when maximising proton production. An explicit phosphate storage reaction was also included in the dFBA. An input reaction for internal phosphate ($PI \rightleftharpoons$) was added to the metabolic model, and the dynamic pool of internal phosphate was tracked in the dFBA. This new reaction was set as the objective when maximising phosphate storage.

When plotting alongside empirical data, the dFBA start time was taken as the spore germination time, 18 hours after inoculation. The initial biomass dry weight was set to 0.3125 g/L following empirical data.

Model parameterisation

Glucose transport-mediated uptake [16, 17] and glucose oxidase [26, 27] kinetic parameters were calculated from empirical data in the literature (Table 2). The concentration of active GOX enzyme [GOX] was fitted to empirical data (Table 1). The other kinetic parameters in the model were fitted to empirical data via a manual fitting routine (Table 1).

Quality of fit assessment and model selection

Akaike Information Criterion (AIC) [20] was used to measure the quality of fit and assess improvement in the model. The AIC was calculated according to

$$AIC = 2k + n \ln \left(\frac{RSS}{n} \right), \quad (11)$$

where k is the number of fitted parameters, n is the number of data-points, and RSS is the residual sum of squares.

Targeted gene deletion of oah and gox

Targeted gene deletion was performed using a previously reported strategy [32]. As this technique requires a pyrG negative strain, the pyrG gene first had to be deleted from ATCC 1015. This was achieved using homologous recombination. ATCC 1015 was transformed with linear DNA containing 2 kb up- and 1.5 kb down-stream flanking regions of the pyrG gene (accession number EHA25155), kindly given by M Kokolski (University of Nottingham). Polyethylene glycol (PEG)-mediated transformation of protoplasts was used [32]. Successful deletions were selected by resistance to 5-fluoroorotic acid (5-FOA) (Fluorochem; Derbyshire, UK) and uridine auxotrophy, and confirmed by PCR and DNA sequencing using primers external to the gene (pyrG_ex_fw and pyrG_ex_rv). The oah and gox genes were identified in the ATCC 1015 genome as accession numbers EHA22250 and EHA27180, respectively. 1.5 kb up- and down-stream flanking regions were cloned from ATCC 1015 gDNA using Phusion HF DNA polymerase (Thermo Fisher Scientific), and the following primers: oah_up_fw, oah_up_rv, oah_down_fw, oah_down_rv, gox_up_fw,

1
2
3
4
5
6
7
8
9
10
11
12
13
14
15
16
17
18
19
20
21
22
23
24
25
26
27
28
29
30
31
32
33
34
35
36
37
38
39
40
41
42
43
44
45
46
47
48
49
50
51
52
53
54
55
56
57
58
59
60
61
62
63
64
65

574 gox_up_rv, gox_down_fw, gox_down_rv. 15-bp tails (underlined) were added to
575 outermost primers for In-Fusion® HD cloning (Clontech; France) into the pc3 vector
576 between the NotI and SpeI restriction sites. To join up- and down-stream fragments
577 together, overlap extension PCR was used with 30-bp overlapping tails (underlined)
578 added to innermost primers. Overlapping fragments were first annealed as follows:
579 50 µl reaction containing 200 ng each fragment, 400 µM dNTPs, HF buffer, and 1 U
580 Phusion HF DNA polymerase run on SOE1 programme (94°C 5 minutes, then 94°C
581 30 seconds, 60°C 90 seconds, 72 °C 90 seconds 10 times, then 10 °C forever). The
582 annealed product was then amplified using outermost primers as follows: 100 µl
583 reaction containing 50 µl first reaction, 1 µM each primer, 400 µM dNTPs, HF buffer
584 and 1 U Phusion HF DNA polymerase run on SOE2 programme (94°C 2 minutes,
585 then 94°C 30 seconds, 60°C 30 seconds, 72°C 90 seconds 35 times, then 72°C 10
586 minutes, 10°C forever). The annealed product was gel purified using the QIAquick
587 gel extraction kit (QIAGEN; Crawley, UK). Transformation was performed using
588 XL10-Gold Ultracompetent cells according to the manufacturer's instructions (Agilent
589 Technologies; Cheshire, UK). Plasmid was isolated using the Wizard® Plus SV
590 minipreps DNA purification kit (Promega; Southampton, UK). Plasmid integrity was
591 confirmed by DNA sequencing. ATCC 1015 ΔpyrG was transformed with the pc3-
592 oah and pc3-gox deletion vectors using the previously reported PEG-mediated
593 protoplast transformation protocol [32]. The gene deletion procedure previously
594 outlined [32] was then followed with minor modifications. 1.5 g/L 5-FOA was used to
595 select for pyrG negative colonies with incubation at 37°C for 3 days. oah and gox
596 knockouts were identified by PCR screening with primers external and internal to the

deletion site (oah_ex_fw, oah_ex_rv, oah_int_fw, oah_int_rv, gox_ex_fw, gox_ev_rv,
gox_int_fw, gox_int_rv). Gene deletion was further confirmed by DNA sequencing of
the region external to the deletion site. To create the Δ oah Δ gox double knockout,
the deletion procedure for gox was applied to ATCC 1015 Δ pyrG Δ oah.

Declarations

Ethics approval and consent to participate

Not applicable.

Consent for publication

Not applicable.

Availability of data and material

The datasets used and/or analysed during the current study are available from the
corresponding author on reasonable request.

Competing interests

The authors declare that they have no competing interests.

Funding

DJU is a student funded by the BBSRC White Rose DTP (BB/J014443/1).

Authors' contributions

DJU, AJW and SMM wrote the manuscript. All authors read and approved the final
manuscript.

Acknowledgements

Not applicable.

References

1. Parshikov IA, Woodling KA, Sutherland JB. Biotransformations of organic compounds mediated by cultures of *Aspergillus niger*. Appl Microbiol Biot. 2015;99:6971-86.
2. Nielsen KF, Mogensen JM, Johansen M, Larsen TO, Frisvad JC. Review of secondary metabolites and mycotoxins from the *Aspergillus niger* group. Anal Bioanal Chem. 2009;395:1225-42.
3. Schuster E, Dunn-Coleman N, Frisvad JC, Van Dijck P. On the safety of *Aspergillus niger*—a review. Appl Microbiol Biot. 2002;59:426-35.
4. Andersen MR, Salazar MP, Schaap PJ, van de Vondervoort PJI, Culley D, Thykaer J, et al. Comparative genomics of citric-acid-producing *Aspergillus niger* ATCC 1015 versus enzyme-producing CBS 513.88. Genome Res. 2011;21:885-897.
5. Cerqueira GC, Arnaud MB, Inglis DO, Skrzypek MS, Binkley G, Simison M, Miyasato SR, Binkley J, Orvis J, Shah P, Wymore F. The *Aspergillus* Genome Database: multispecies curation and incorporation of RNA-Seq data to improve structural gene annotations. Nucleic Acids Res. 2014;42:705-710.
6. Knuf C, Nielsen J. Aspergilli: systems biology and industrial applications. Biotechnol J. 2012;7:1147-55.
7. Chinese citric acid industry begins to consolidate. In: Analysis. F.O. Licht Renewable Chemicals. 2011. <http://stage.renewablechemicals.agranet.com/chinese-citric-acid-industry-begins-to-consolidate/>. Accessed 6 July 2017.

- 640 8. Citric Acid. In: Chemical Economics Handbook. IHS. 2015.
641 <https://www.ihs.com/products/citric-acid-chemical-economics-handbook.html>.
642 Accessed 6 July 2017.
- 643 9. Dhillon GS, Brar SK, Kaur S, Verma M. Screening of agro- industrial wastes for
644 citric acid bioproduction by *Aspergillus niger* NRRL 2001 through solid state
645 fermentation. J Sci Food Agr. 2013;93:1560-1567.
- 646 10. Papagianni M. Advances in citric acid fermentation by *Aspergillus niger*:
647 Biochemical aspects, membrane transport and modeling. Biotechnol Adv.
648 2007;25:244-63.
- 649 11. Orth JD, Thiele I, Palsson BØ. What is flux balance analysis? Nat Biotechnol.
650 2010;28:245-8.
- 651 12. Max B, Salgado JM, Rodríguez N, Cortés S, Converti A, Domínguez JM.
652 Biotechnological production of citric acid. Braz J Microbiol. 2010;41:862-75.
- 653 13. Andersen MR, Nielsen ML, Nielsen J. Metabolic model integration of the
654 bibliome, genome, metabolome and reactome of *Aspergillus niger*. Mol Syst Biol.
655 2008;4:178.
- 656 14. Andersen MR, Lehmann L, Nielsen J. Systemic analysis of the response of
657 *Aspergillus niger* to ambient pH. Genome Biol. 2009;10:R47.
- 658 15. Schneider KD, Van Straaten P, Orduña D, Mira R, Glasauer S, Trevors J, Fallow
659 D, Smith PS. Comparing phosphorus mobilization strategies using *Aspergillus niger*
660 for the mineral dissolution of three phosphate rocks. J Appl Microbiol. 2010;108:366-
661 74.

16. Torres NV, Riol-Cimas JM, Wolschek M, Kubicek CP. Glucose transport by *Aspergillus niger*: the low-affinity carrier is only formed during growth on high glucose concentrations. Appl Microbiol Biot. 1996;44:790-4.
17. Papagianni M, Matthey M. Modeling the mechanisms of glucose transport through the cell membrane of *Aspergillus niger* in submerged citric acid fermentation processes. Biochem Eng J. 2004;20:7-12.
18. Gonzalez JE, Long CP, Antoniewicz MR. Comprehensive analysis of glucose and xylose metabolism in *Escherichia coli* under aerobic and anaerobic conditions by ¹³C metabolic flux analysis. Metab Eng. 2017;39:9-18.
19. Legiša M, Kidrič J. Initiation of citric acid accumulation in the early stages of *Aspergillus niger* growth. Appl Microbiol Biot. 1989;31:453-7.
20. Akaike H. Information theory and an extension of the maximum likelihood principle. In: Petrov BN, Csáki F. 2nd International Symposium on Information Theory. Budapest: Akadémiai Kiadó; 1973. p. 267–281.
21. Capuder M, Šolar T, Benčina M, Legiša M. Highly active, citrate inhibition resistant form of *Aspergillus niger* 6-phosphofructo-1-kinase encoded by a modified *pfkA* gene. J Biotechnol. 2009;144:51-7.
22. De Jongh WA, Nielsen J. Enhanced citrate production through gene insertion in *Aspergillus niger*. Metab Eng. 2008;10:87-96.
23. Nishi A. Role of polyphosphate and phospholipid in germinating spores of *Aspergillus niger*. J Bacteriol. 1961;81:10.
24. Huson DH, Richter DC, Rausch C, DeZulian T, Franz M, Rupp R. Dendroscope: An interactive viewer for large phylogenetic trees. BMC Bioinformatics. 2007;8:1.

- 685 25. Ruijter GJ, van de Vondervoort PJ, Visser J. Oxalic acid production by
686 *Aspergillus niger*: an oxalate-non-producing mutant produces citric acid at pH 5 and
687 in the presence of manganese. Microbiology. 1999;145:2569-76.
- 688 26. Kalisz HM, Hecht HJ, Schomburg D, Schmid RD. Effects of carbohydrate
689 depletion on the structure, stability and activity of glucose oxidase from *Aspergillus*
690 *niger*. BBA-Protein Struct M. 1991;1080:138-142.
- 691 27. Swoboda BE, Massey V. Purification and properties of the glucose oxidase from
692 *Aspergillus niger*. J Biol Chem. 1965;240:2209-15.
- 693 28. Wilson R, Turner APF. Glucose oxidase: an ideal enzyme. Biosens Bioelectron.
694 1992;7:165-85.
- 695 29. Rodríguez H, Fraga R. Phosphate solubilizing bacteria and their role in plant
696 growth promotion. Biotechnol Adv. 1999;17:319-39.
- 697 30. Chuang CC, Kuo YL, Chao CC, Chao WL. Solubilization of inorganic phosphates
698 and plant growth promotion by *Aspergillus niger*. Biol Fert Soils. 2007;43:575-584.
- 699 31. Lu H, Cao W, Ouyang L, Xia J, Huang M, Chu J, Zhuang Y, Zhang S, Noorman
700 H. Comprehensive reconstruction and *in silico* analysis of *Aspergillus niger*
701 genome-scale metabolic network model that accounts for 1210 ORFs. Biotechnol
702 Bioeng. 2017;114:685-95.
- 703 32. Delmas S, Llanos A, Parrou JL, Kokolski M, Pullan ST, Shunburne L, Archer DB.
704 Development of an unmarked gene deletion system for the filamentous fungi
705 *Aspergillus niger* and *Talaromyces versatilis*. Appl Environ Microb. 2014;80:3484-7.

Table 1. Parameters fitted to our empirical data.

Parameter	Description	Value
$v_{Pe,max}$ (mmol gDW ⁻¹ h ⁻¹)	External phosphate maximum input rate ^a	0.08
K_{Pe} (mM)	External phosphate Michaelis constant	0.0333
$v_{P,max}$ (mmol gDW ⁻¹ h ⁻¹)	Internal phosphate maximum input rate	0.0008
K_P (mM)	Internal phosphate Michaelis constant	0.0833
v_{G1} (mmol gDW ⁻¹ h ⁻¹)	External glucose passive uptake rate	$0.00031419 \times [\text{GLC}]^b$
v_{X1} (mmol gDW ⁻¹ h ⁻¹)	External xylose passive uptake rate	$0.00033 \times [\text{XYL}]^c$
$v_{X2,max}$ (mmol gDW ⁻¹ h ⁻¹)	External xylose high-affinity transport maximum rate	0.2
K_{X2} (mM)	External xylose high-affinity transport Michaelis constant	3.33
$v_{X3,max}$ (mmol gDW ⁻¹ h ⁻¹)	External xylose low-affinity transport maximum rate	2.5
K_{X3} (mM)	External xylose low-affinity transport Michaelis constant	3.33
[GOX] (mg gDW ⁻¹)	Concentration of external glucose oxidase enzyme	0.1
v_{CIT} (mmol gDW ⁻¹ h ⁻¹)	Citric acid output rate constraint ^d	0.12
v_{OXAL} (mmol gDW ⁻¹ h ⁻¹)	Oxalic acid output rate constraint	0.01

^aExternal phosphate input rate changed 8 hours after the dFBA start time to 0.015 mmol gDW⁻¹ h⁻¹ if initial pH 2 or 0.004 mmol gDW⁻¹ h⁻¹ if initial pH 7. ^b[GLC] is concentration of external glucose in mM. ^c[XYL] is concentration of external xylose in mM. ^dCitric acid output rate constraint changed to 0.016 mmol gDW⁻¹ h⁻¹ if initial pH above 2.

Table 2. Parameters set to empirical values from the literature.

Parameter	Description	Value	References
$v_{G2,max}$ (mmol gDW ⁻¹ h ⁻¹)	External glucose high-affinity transport maximum rate	0.186	[16, 17]
K_{G2} (mM)	External glucose high-affinity transport Michaelis constant	0.26	[16, 17]
K_{i2} (mM)	External glucose high-affinity transport citrate inhibition constant	933	[16, 17]
$v_{G3,max}$ (mmol gDW ⁻¹ h ⁻¹)	External glucose low-affinity transport maximum rate	2.706	[16, 17]
K_{G3} (mM)	External glucose low-affinity transport Michaelis constant	3.67	[16, 17]
K_{i3} (mM)	External glucose low-affinity transport citrate inhibition constant	233.21	[16, 17]
$v_{GOX,max}$ (mmol gDW ⁻¹ h ⁻¹)	Glucose oxidase (GOX) maximum reaction rate	$27.48 \times [\text{GOX}]^a$	[26]
K_{GOX} (mM)	Glucose oxidase (GOX) Michaelis constant	33	[26, 27]

^a[GOX] is concentration of external glucose oxidase enzyme in mg gDW⁻¹ and was fitted to empirical data (Table 1).

Table 3. Acid constants for Equation 10.

Acid species	K_1	K_2	K_3
Citric acid	$10^{-3.128}$	$10^{-4.761}$	$10^{-6.396}$
Gluconic acid	$10^{-3.7}$	0	0
Acetic acid	$10^{-4.757}$	0	0
Malic acid	$10^{-3.459}$	$10^{-5.097}$	0
Succinic acid	$10^{-4.207}$	$10^{-5.636}$	0
Lactic acid	$10^{-3.86}$	0	0
Oxalic acid	$10^{-1.252}$	$10^{-4.266}$	0

Table 4. AIC scores for model selection.

Additional parameters	Number of fitted parameters	AIC score
None	5	438
Nucleic acid component of biomass equation	6	416
Phospholipid component of biomass equation	6	422
Nucleic acid and phospholipid components of biomass equation	7	393
Nucleic acid and phospholipid components of biomass equation, and citric acid output constraint	8	300

Table 5. Primers used in this work.

Primer	Nucleotide sequence (5' to 3')
pyrG_ex_fw	CTTTGCAGGTGTGGCTGAAC
pyrG_ex_rv	ACAGCAGTGCTTATCTGCGA
oah_up_fw	<u>ACCGCGGTGGCGGCCGCGCTGTGTCCATACCATCAATCC</u>
oah_up_rv	<u>GAATGTTGCAGACAGACAGAAAGCAAAAGAGCAGGCAGTAGTAAGCAA</u> GAAT
oah_down_fw	<u>TCTTTCTTATTCTTGCTTACTACTGCCTGCTCTTTTGCTTTCTGTCTGTC</u> TGC
oah_down_rv	<u>CGGGGGATCCACTAGTTCTCCTCTTCCCCTGCCTTT</u>
gox_up_fw	<u>ACCGCGGTGGCGGCCGCGAGATGGCAATTTCCGCGAC</u>
gox_up_rv	<u>GAATATTCGAGGATTGTGGGAGAGACAGCGCGTGCAAACCTCACCACC</u> AAG
gox_down_fw	<u>CTGTCTTGACCTTGGTGGTGAGTTTGCACGCGCTGTCTCTCCCACAAT</u> CC
gox_down_rv	<u>CGGGGGATCCACTAGTCTACGCTCATGTCCTGGTCC</u>
oah_ex_fw	TAAGGCTACCCAACCCACCC
oah_ex_rv	GCTTATCTAGGCCCTGCTG
oah_int_fw	ACCCAACCACACCATCCTTC
oah_int_rv	ACCCAGTTCCCCACTAACAC
gox_ex_fw	CACTATCGCCAAGCAGGGAT
gox_ex_rv	AAGGTCTCGTTGAAGGTGGC
gox_int_fw	AGCAACCAGCCTTTCCTCTC
gox_int_rv	CCCAGTTCCAGCCCTCATTT

Figure legends

Figure 1. Citric acid production commences upon a diauxic growth switch. Empirical data plotted is the mean average of 4 biological replicates and error bars represent standard deviation. Citric acid data are normalised to reflect the amount produced.

A) Change in biomass dry weight (g/L) over time. **B)** Change in external citric acid concentration (g/L) over time.

Figure 2. Comparing empirical and *in silico* data in response to varying phosphate.

Markers represent empirical data and lines represent *in silico* data. Green circles and dashed-dotted lines correspond to 0.05 g/L phosphate. Purple triangles and dashed lines correspond to 0.09 g/L phosphate. Brown squares and solid lines correspond to 0.17 g/L phosphate. Empirical data plotted is the mean average of 4 biological replicates and error bars represent standard deviation. Citric acid data are normalised to reflect the amount produced. *In silico* data-points are one per minute.

A) Change in biomass dry weight (g/L) over time. **B)** Change in external phosphate concentration (g/L) over time. **C)** Change in external citric acid concentration (g/L) over time. **D)** Change in external glucose concentration (g/L) over time.

Figure 3. Simulating citric acid fermentation by dynamic flux balance analysis. A schematic showing the decision process implemented in the dFBA model.

Figure 4. Comparing empirical and *in silico* data in response to different carbon sources. Markers represent empirical data and lines represent *in silico* data. Green

circles and solid lines correspond to glucose. Purple triangles and dashed lines correspond to xylose. Empirical data plotted is the mean average of 4 biological replicates and error bars represent standard deviation. Citric acid data are normalised to reflect the amount produced. *In silico* data-points are one per minute. **A)** Change in biomass dry weight (g/L) over time. **B)** Change in external phosphate concentration (g/L) over time. **C)** Change in external citric acid concentration (g/L) over time. **D)** Change in external carbon source concentration (g/L) over time.

Figure 5. Change in polyphosphate levels during citric acid fermentation. Empirical data plotted is the mean average of 3 biological replicates and error bars represent standard deviation.

Figure 6. Comparing empirical and *in silico* data in response to Δoah and Δgox knockouts. Markers represent empirical data and lines represent *in silico* data. Green circles and solid lines correspond to $\Delta oah \Delta gox$. Purple triangles and dashed-dotted lines correspond to Δoah . Brown squares and dashed lines correspond to Δgox . Blue diamonds and dotted lines correspond to $\Delta pyrG$ control. Empirical data plotted is the mean average of 4 biological replicates and error bars represent standard deviation. Citric acid data are normalised to reflect the amount produced. *In silico* data-points are one per minute. **A)** Change in external citric acid concentration (g/L) over time. **B)** Change in external oxalic acid concentration (g/L) over time. **C)** Change in external gluconic acid concentration (g/L) over time. **D)** Change in external phosphate concentration (g/L) over time.

Table S1. Biomass equation parameters altered to fit empirical data.

Compound	Before fitting (mmol gDW ⁻¹ h ⁻¹)	After fitting (mmol gDW ⁻¹ h ⁻¹)
AMP	-0.01402222	-0.0046740733
GMP	-0.01688834	-0.0056294467
CMP	-0.01402222	-0.0046740733
UMP	-0.01117424	-0.0037247467
DAMP	-0.00193736	-0.0006457867
DCMP	-0.00201544	-0.0006718133
DTMP	-0.00193736	-0.0006457867
DGMP	-0.00201544	-0.0006718133
PC	-0.015312	-0.005104
PS	-0.000359	-0.0001196667
PE	-0.034807	-0.0116023333
GL	-0.46	-0.9030928715
ADP	71.60986992	71.5025795733
PI	71.60986992	71.5025795733
ATP	-71.60986992	-71.5025735267
H2O	-69.08036756	-69.0511151733

Table S2. Putative phosphate transporters in ATCC 1015. Top BLASTP hits with phosphate transporters in SwissProt database are given.

ATCC 1015 locus tag	GenBank accession	Top BLASTP hit (SwissProt)	Identity (%)	E-value
ASPNIDRAFT_173247	EHA22558	P15710.1	37	4e-130
ASPNIDRAFT_190334	EHA20653	P25297.2	34	2e-90
ASPNIDRAFT_121846	EHA27663	Q7RVX9.2	61	0.0
ASPNIDRAFT_52154	EHA22720	O42885.2	29	2e-42
ASPNIDRAFT_42307	EHA25335	Q9S735.1	27	6e-12
ASPNIDRAFT_175394	EHA23128	Q8H074.1	25	2e-26
ASPNIDRAFT_206238	EHA26306	P27514.2	41	0.0
ASPNIDRAFT_35379	EHA27197	Q8H074.1	24	2e-22

Supplementary Figure legends

Figure S1. Phylogenetic tree of putative phosphate transporters in ATCC 1015.

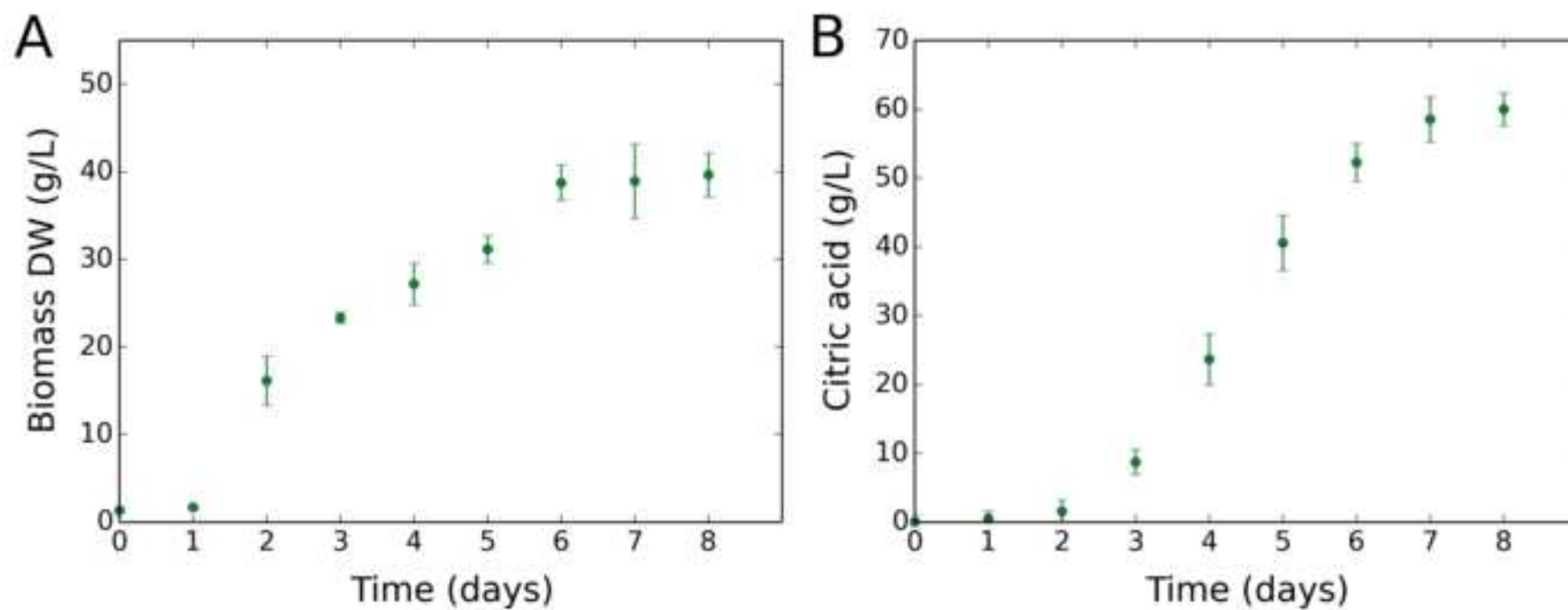
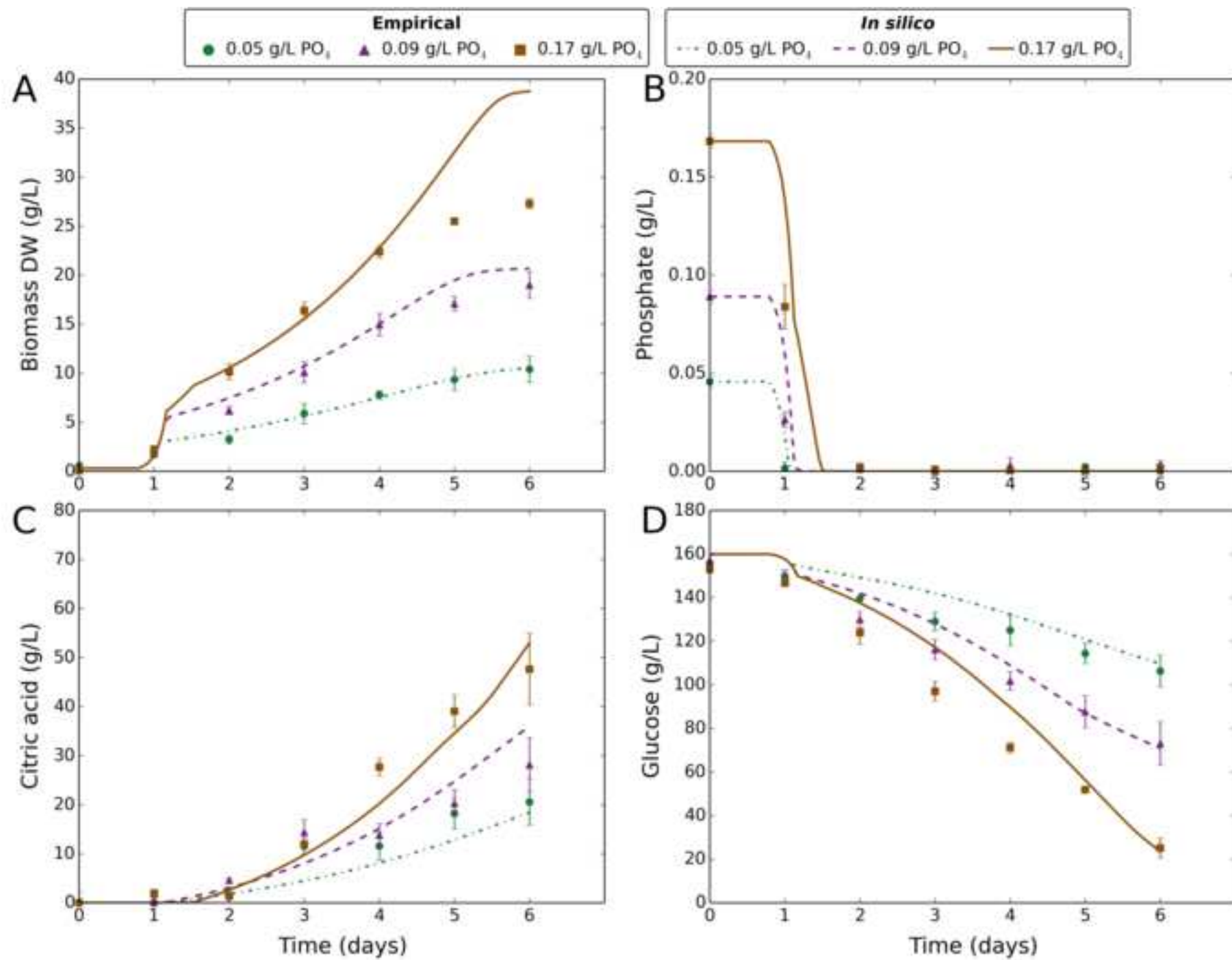


Figure2

[Click here to download Figure Figure2.png](#)

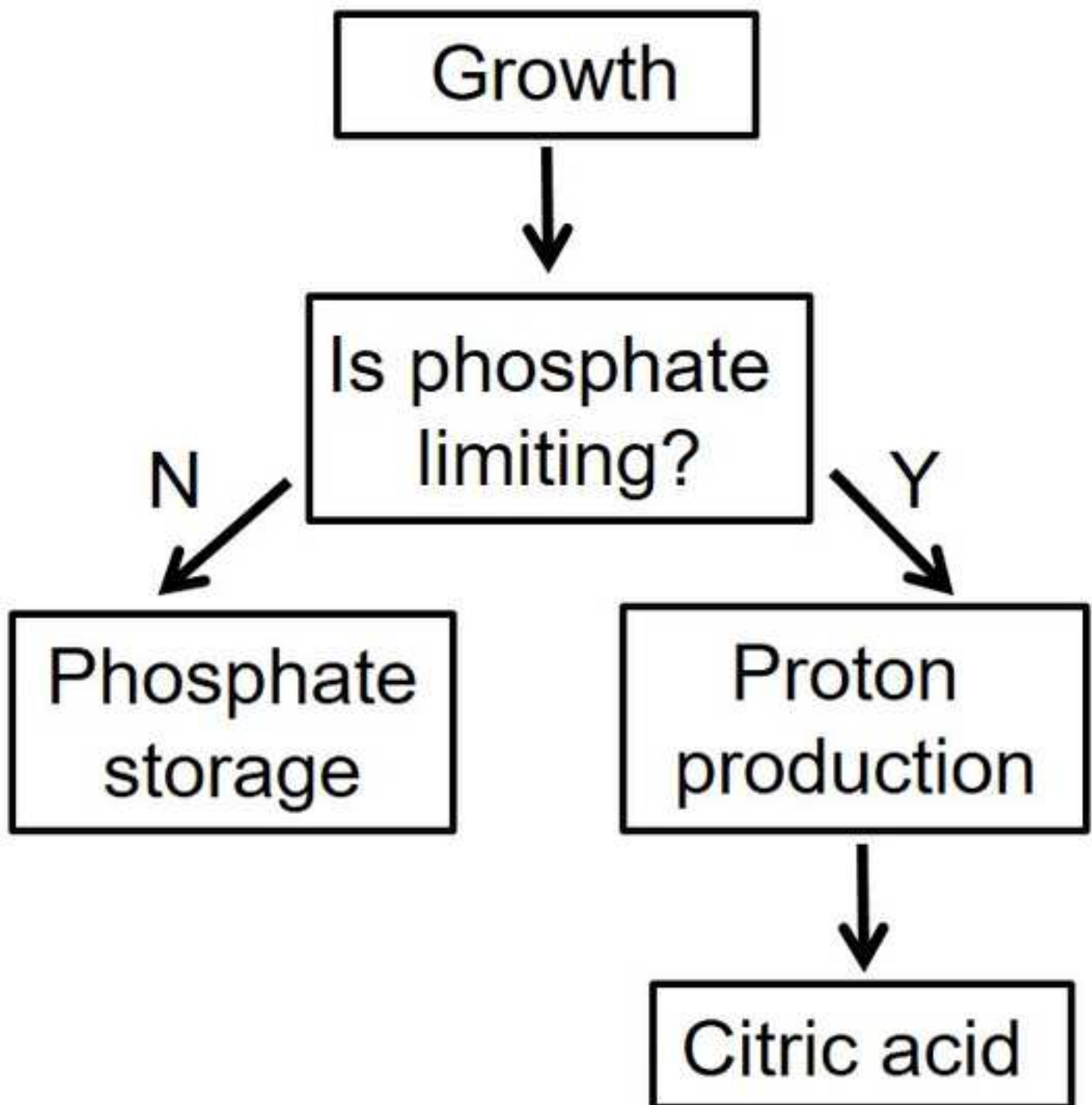
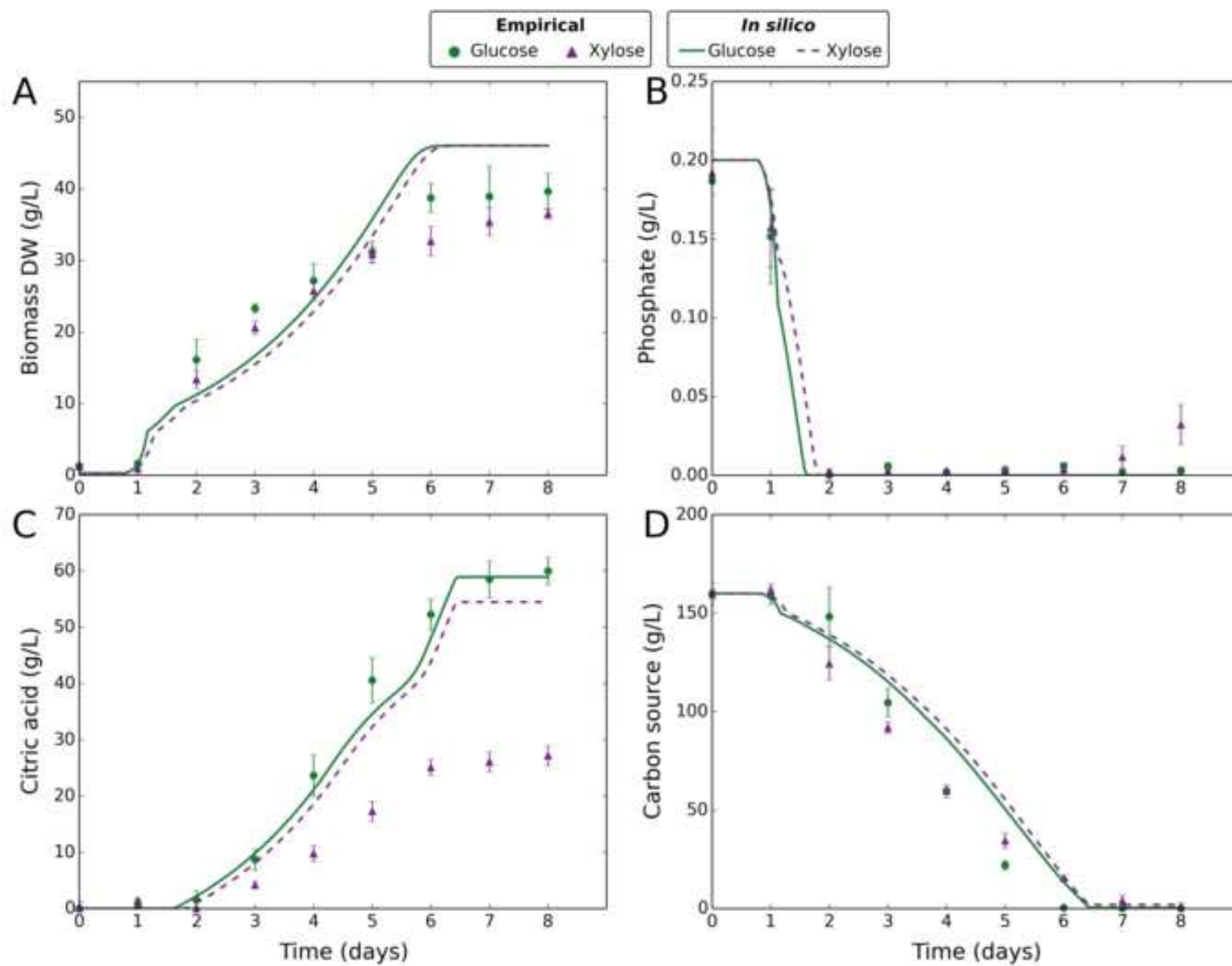


Figure4

[Click here to download Figure Figure4.png](#)

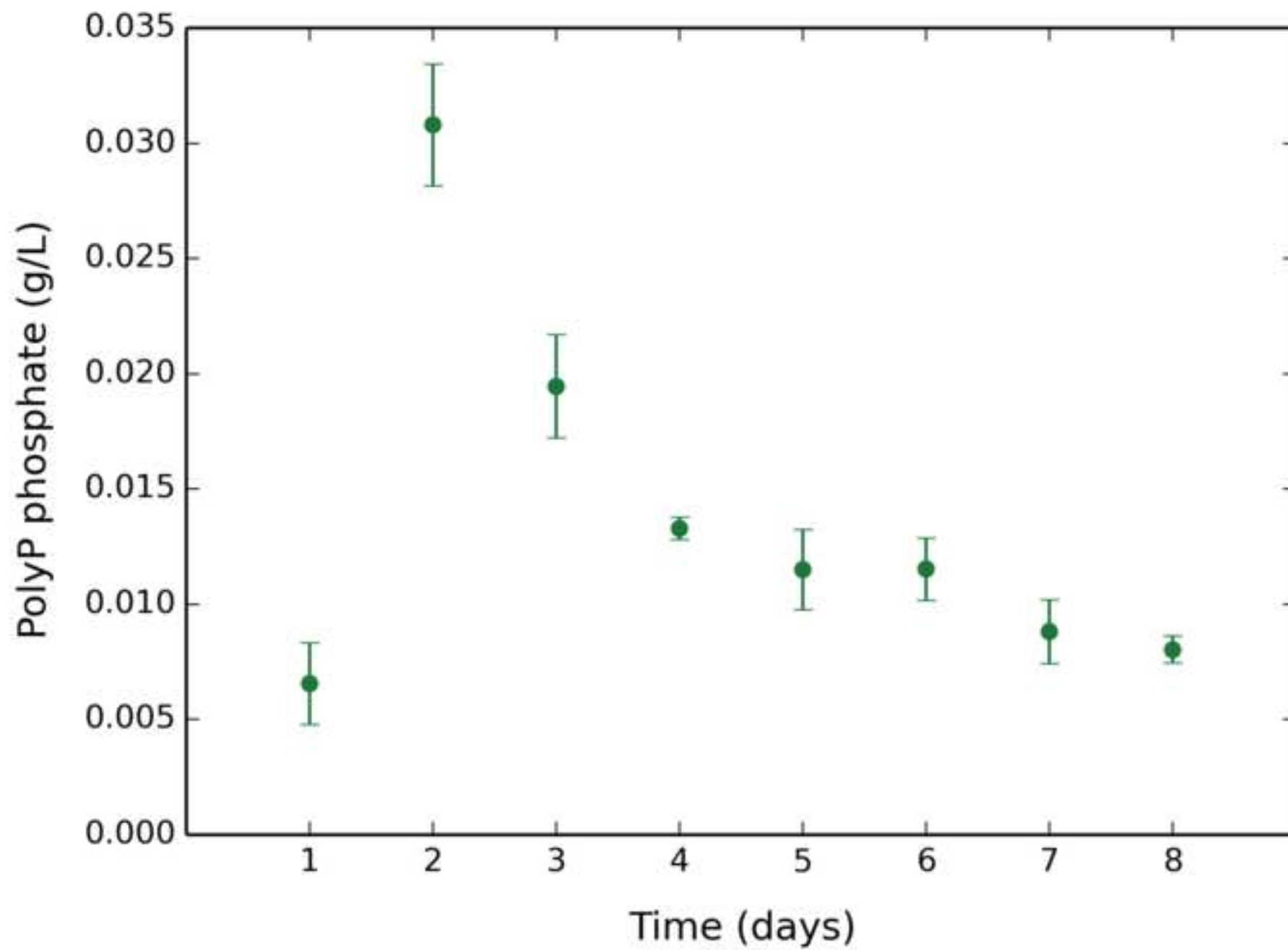
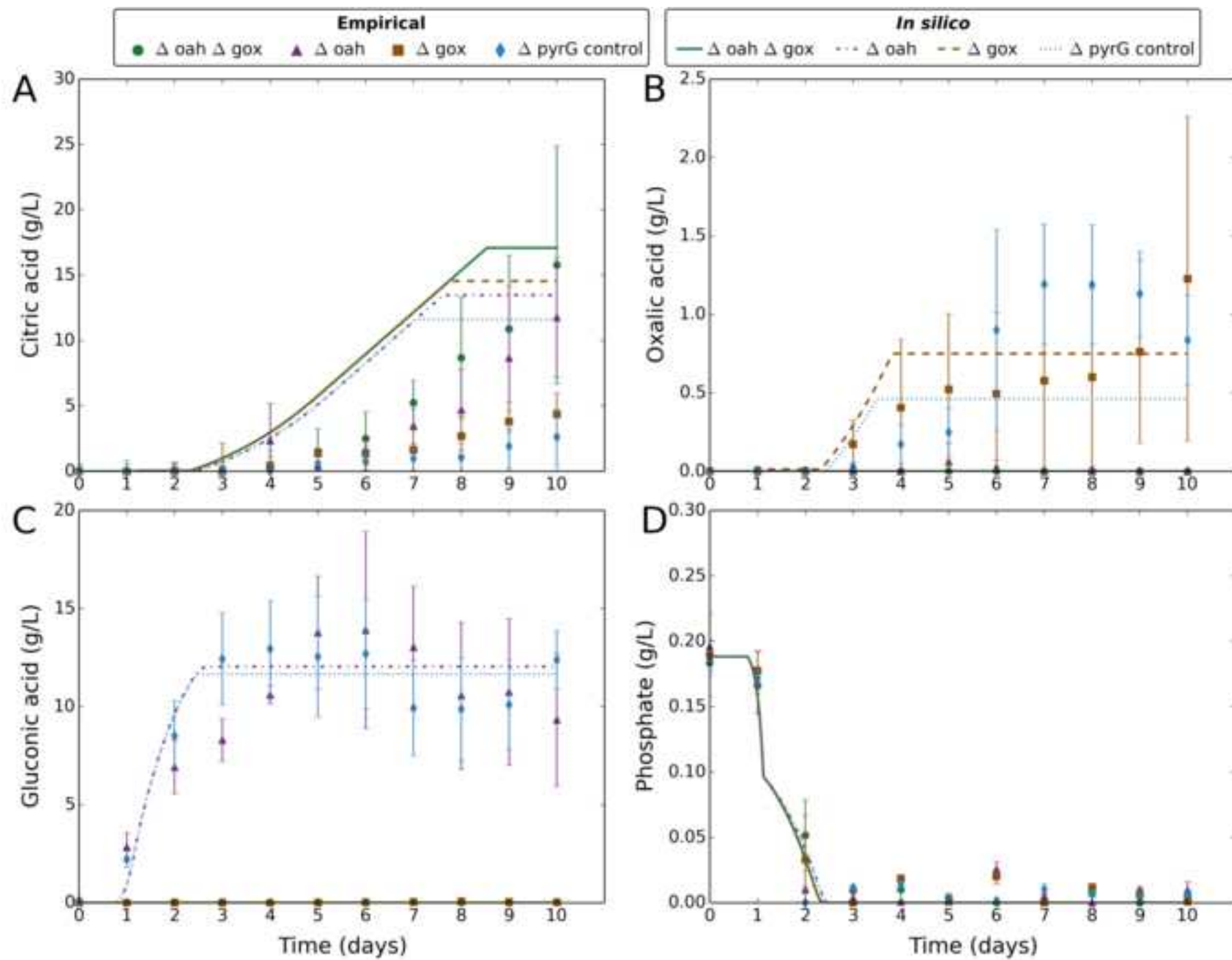



Figure6

[Click here to download Figure Figure6.png](#)



Click here to access/download
Supplementary Material
FigureS1.tiff

